

# Tannic Acid-Terminated Poly(Propylene Oxide) as Efficient Dispersant for Multi-Walled Carbon Nanotube to Prepare Highly Conductive Composites

Pei-Ni Song<sup>1</sup>, Jin-Long Hong<sup>2\*</sup>

<sup>1</sup>Department of Materials and Optoelectronic Science, National Sun Yat-sen University

<sup>2\*</sup>Department of Materials and Optoelectronic Science, National Sun Yat-sen University, Kaohsiung, Taiwan 80424, ROC

**Abstract**—In this study, multi-functional tannic acid (TA) was incorporated with soft poly(propylene oxide) (PPO) chain to result in a TA-terminated JTA polymer, in which the TA terminals impart reversible aromatic  $\pi$ - $\pi$  and hydrogen bond (H bond) interactions to JTA polymer. Moreover, the aromatic TA terminals of JTA can preferably bind to the surface carbon rings of multi-walled carbon nanotubes (MWCNTs) to result in JCTx composites containing large amounts (up to 96 wt%) of MWCNTs. The sorption isotherm study indicated a two-step sorption mechanism of the sorbed JTA on MWCNT. Dependent on the MWCNT content, JCTx composites can be healable elastomers with high fracture strain (up to 700%) or plastics with outstanding conductivity (up to  $1.21 \times 10^6$  m-1). Experimental mechanical modulus and conductivity of JCTx also were approached by the theoretical Kolarik model and scaling law, respectively. The result was explained in term of morphological arrangement of the MWCNT, evaluated from scanning and transmission) electron microscopies in JTA matrix. This study provided theoretical evaluation of highly MWCNT-loaded composites.

**Keywords**—Tannic acid, MWCNT, carbon material dispersion,  $\pi$ - $\pi$  stacking, hydrogen bonding, conductive composite, Kolarik model, scaling law.

## I. INTRODUCTION

Molecular engineering using delicate design and testing of molecular structures and interactions enables the fabrication of advanced materials with different application fields. Given the extraordinary mechanical, electrical, and thermal properties, carbon nanotubes (CNTs) provided versatile routes for the preparations of advanced materials, among them, polymer/CNT nanocomposites<sup>1,2</sup> were studied frequently despite the existing difficulty in fabricating homogenous composite products. Primarily, dispersing CNTs without destroying the superior mechanical and electrical properties, with some notable exceptions (<10%)<sup>3-5</sup>, were hampered by the lack of effective method in dispersing large amounts of CNTs. Primarily, it is difficult to disperse nanotubes in water due to the repulsive interactions<sup>6-8</sup> between nanotubes and water. Moreover, the large attractive interparticle potential between the nanoscale tubes<sup>9,10</sup> caused the easy formation of aligned aggregated tubes. Several methods have been developed to disperse CNTs<sup>11-13</sup> previously, nevertheless, the amounts of nanotubes incorporated in the polymer composites are limited ( $\leq 10$  wt%) due to the preferable aggregation tendency of nanotubes in the polymer solutions.

Introducing conductive materials into insulating hosts<sup>14-16</sup> always is an attracting topic because of the scientific and practical importance. The electrical conductivity of nanotubes can reach  $10^6$  S m<sup>-1</sup>, but polymer matrices usually are poor in conductivity with values between  $10^{-16}$  and  $10^{-12}$  S m<sup>-1</sup>. Adding small amounts of nanotubes to polymer matrices significantly increased the conductivity<sup>17-24</sup> (to  $10^{-6}$  S m<sup>-1</sup>, approximately), which stimulated the practical applications of polymer/carbon nanotube (PCNT) composites in electronics, sensors, and actuators, as well as many others<sup>25,26</sup> in the electronics industry. The critical concentration<sup>27,28</sup>, known as percolation threshold, at which conductive networks start to form is inversely related to the aspect ratio (length per diameter) of the dispersed nanomaterials. Regarding the high aspect ratio of nanotubes, PCNT nanocomposites generally exhibit extremely low (< 0.5 wt%) percolation thresholds<sup>29-33</sup>. Experimental and theoretical approaches for the percolation thresholds indicated that conductivity of PCNTs was limited by the potential barriers between nanotubes and polymer because the surfaces of the nanotube bundles always were covered by polymer coatings.

Besides conductivity, a percolation threshold, known as mechanical percolation, also was observed in the mechanical tests of PCNTs. Previous study<sup>34,35</sup> had interpreted the high levels of modulus in reinforced composites and nanocomposites by mechanical percolation. CNTs show Young's moduli of around 1000 GPa as well as tensile strengths in range from 10 to 50 GPa<sup>36</sup>. The excellent mechanical performance as well as the extraordinary physical properties, such as high aspect ratios and large surface areas, justifies their beneficial role in PCNTs. Again, the advantage of nanotubes was only realized when they are uniformly dispersed in the polymer matrices, because that they tend to aggregate/agglomerate<sup>37</sup> seriously in the processing solution step. Therefore, more promising PCNTs<sup>38-49</sup> with low (e.g. 0.8 wt%), medium (e.g. 10 wt%) and high (e.g. 33 wt%) nanotube content had been previously attempted. Among them, poly(acrylic acid)/poly(ethylene oxide)-poly(propylene oxide)-poly(ethylene oxide)<sup>49</sup> (PAA/F108) was used as excellent dispersant of CNT to result in PCNT with a high amount (33 wt%) of CNT. The facile hydrogen bond (H bond) interactions between carboxylic acids in PAA and over the active surface of CNT are responsive for the homogeneity of the resulting PCNTs.

As a universal environmental organic molecule, tannic acid (TA)<sup>50,51</sup> was previously used as effective dispersant for CNTs. The enriched aromatic rings and phenolic hydroxyl OH groups of TA are responsible for the effective dispersion of CNTs and accordingly, a two-stage sorption mechanism<sup>50</sup> was proposed: the TA molecules were adsorbed first onto the surfaces of CNTs with the aromatic rings binding to the surface carbon rings of CNT via the aromatic  $\pi$ - $\pi$  interactions, forming a monolayer in the interface, which further adsorbed the dissolved TA molecules by the self-interacting H bonding and other possible polar interactions. The adsorbed TA molecules increased the steric repulsion between individual CNT, which then acted to disperse the loose CNT aggregates to result in the stabilization of CNTs in the TA solution. The sorption and suspending process also was examined by transmission electron (TEM) microscopy, providing further evidence for the above sorption mechanism.

In this study, we designed and synthesized a TA-terminated poly(propylene oxide) (PPO) of JTA (Scheme 1), which turned out to be effective sorbent for MWCNT exclusively binding to various amount of MWCNT to result in JCTx (x: wt% of MWCNT, ranging from 1 to 96) composites with high conductivity (from  $1.20 \times 10^{-3}$  to  $1.21 \times 10^6 \text{ S m}^{-1}$ ) and excellent mechanical properties to be studied with. The multi-functional JTA polymer is an elastomer due to its unique molecular feature that the soft PPO chain is the mobile and stretchable part while the aromatic  $\pi$ - $\pi$  and H bond interaction sites of TA terminals provide mechanical strength susceptible to external deformation. TA terminals of JTA also imparted exclusive aromatic  $\pi$ - $\pi$  interactions to the surface carbon rings of MWCNT, rendering stretchable elastomer (while MWCNT content is low ( $\leq 40$  wt%)) or hard conductive plastics (while MWCNT content is higher than 40 wt%) with interesting mechanical and conductive properties to be studied with. Rather than previous study<sup>52,53</sup> always concentrated on PCNTs with concentration below percolation threshold, the JCTx composites provided us the opportunity to approach the experimental mechanical modulus (E) and conductivity with theoretical Kolarik model<sup>54</sup> and scaling law<sup>55</sup>, respectively, at concentration well beyond percolation threshold. Starting from the sorption study in the solution state, a two-stage sorption model was proposed to illustrate the interaction between MWCNTs and JTA. Mechanical and conductive properties of the solid composites also were correlated with the morphological arrangement of MWCNTs in JTA matrix evaluated from scanning (SEM) and transmission (TEM) electron microscopies. This study therefore provided theoretical background on the highly MWCNT-loaded PCNTs.

## II. EXPERIMENTAL

### 2.1 Materials

Amine-terminated PPO (Jeffamine,  $M_n=4,684$  g/mol, Sigma-Aldrich) and hexamethylene diisocyanate (HDI,  $M_n=168$  g/mol, Acros) and TA ( $M_n=1,701$  g/mol, Acros) were directly used without purification. MWCNT was purchased from Golden Innovation Business Co., Ltd, which was claimed to have inner and outer diameters of 10 nm and 20 nm, and 1 to 2  $\mu\text{m}$  in length, respectively. Preparation method is Model equation and parameter definition (CVD). *N,N*-dimethyl formamide (DMF) was refluxed over  $\text{CaH}_2$  for two days in prior to distillation for use.

## 2.2 Preparation of JTA

The JTA was synthesized by a two-step reaction procedure (Scheme 1). Briefly, solution of Jeffamine (5g, 1.07 mmol) and HDI (0.38 g, 2.25 mmol) in dry DMF (25 mL) were heated at 70 °C for 3 hr to result in homogeneous JHDI solution. A small portion of the solution was taken and extracted by hexane before being precipitated from distilled water to obtain JHDI for analysis. Afterwards, TA (4.55 g, 2.68 mmol) was added to the solution mixture and the reaction was continued at 80 °C for another 24 hr. The reaction mixture was then cooled to room temperature and extracted by hexane for several times before being precipitated from distilled water. The slurry-like product was filtered and dried at 70 °C for 24 hr under vacuum.

## 2.3 Preparation of conductive composite film

Calculated amounts of JTA and MWCNT were sonicated in DMF (5 mL) for 1 hr to ensure complete dispersion of MWCNT. The resulting homogeneous solution was then dried under vacuum for 24 hr to result in JCTx composite films for study.

## 2.4 Sorption and Stabilization Experiments

Sorption isotherms were obtained using a batch equilibration technique at 25°C. Two hundred milligrams of MWCNTs were added into 20 mL vials with different JTA concentrations of 0.8, 9, 44.5, 89, 445 and 890 mg/L. The whole vial was sonicated for 1 hr before standing still for equilibration for 7 days, and the resulting supernatants, the stable suspensions possibly with dispersed individual nanotubes, were taken out and measured with UV-Vis spectrometer (Jasco V-770, USA) at 800 nm. Measurement at 800 nm had been used to quantify MWCNTs in DMF phase. Preliminary experiments indicated that the absorbances at 800 nm are the same for solutions after being sonicated for 0.5 hr and 3 hr, thus, the suspended MWCNTs in the supernatants after sonication were considered to be stable in JTA solutions.

## 2.5 Characterizations

<sup>1</sup>H NMR spectra were measured using a Varian Unity VXR-500 MHz spectrometer (McKinley Scientific, Sparta, NJ, USA), with *d*<sub>6</sub>-DMSO as the solvent and tetramethylsilane (TMS) as the external standard. A mass spectrum was obtained by using a Bruker Daltonics Autoflex III MalDI-ToF mass spectrometer with *trans*-2-[3-(4-*tert*-butylphenyl)-2-methyl-2-propenylidene] malononitrile (DCTB) as matrix material. The number and weight-average molecular weights ( $M_n$  and  $M_w$ ) and polydispersity (PDI) were determined from gel permeation chromatography (GPC) using a Waters 510 high-performance liquid chromatography system and DMF at 45 °C as the eluent (flow rate: 0.6 mL min<sup>-1</sup>). The electric properties were determined at room temperature by an LCR Tonghui TH 2829 meter at 1 kHz with each data point as the average value of five measurements. Bright field TEM images of mass-thickness contrast were obtained using a Jeol JEM 2100 TEM spectrometer at an accelerating voltage of 200 kV. The samples were prepared by air-drying a drop of the suspensions onto a copper TEM grid. SEM images were obtained using a Jeol JSM 6700F microscope operated at 10 kV.

## III. RESULT AND DISCUSSION

As illustrated in Scheme 2, the preparation of the desired polymer JTA required the preliminary synthesis of a key precursor JHDI. The reaction of the amino terminals of Jeffamine with excess (2.1 eq) HDI resulted in an isocyanate-terminated JHDI, which under attack of the phenolic OH groups of TA (2.5 eq) produced the desired JTA for study. To examine the efficiency of the applied end-capping reaction, the <sup>1</sup>H NMR spectrum of JTA, including all peak assignments, was compared with those of *d*<sub>6</sub>-DMSO, Jeffamine and JHDI in Figure 1. The average HDI unit per Jeffamine chain of JHDI was determined from the integration ratio between resonance protons H<sub>e</sub> at 2.89 ppm and H<sub>a,d</sub> at 0.93-1.14 ppm. Here, the peak intensity of protons H<sub>e</sub> was used to calculate the fraction of H<sub>d</sub> in the overlapped H<sub>a,d</sub> peaks as H<sub>e</sub> and H<sub>d</sub> belong to the same hexamethyl unit of HDI terminals with a fixed ratio of 1 to 2. Accordingly, the average HDI unit per Jeffamine chain of JHDI is 1.93. Likewise deduction, from the integration ratio between protons H<sub>h1+h2+j1+j2</sub> and H<sub>a,d</sub>, resulted in an average 1.89 TA terminals per JTA chain. The resolved  $M_n$ s (5,009 g/mol for JHDI and 8,289 g/mol for JTA) listed in Table 1 are comparable with those determined from MalDI-ToF mass spectroscopy but are smaller than those from the GPC analysis. The high molecular weights determined from GPC can only be regarded as reference values because GPC analysis involved only excluded volume of the polymer, rather than real molecular weights, in DMF eluent.

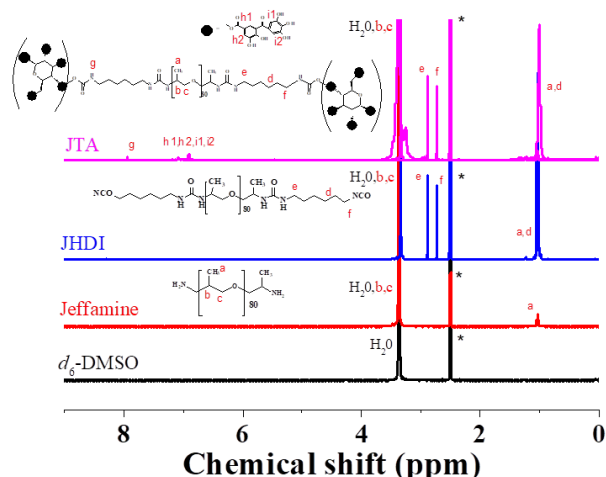


FIGURE 1.  $^1\text{H}$  NMR spectra of  $d_6$ -DMSO, Jeffamine, JHDI and TA-terminated JTA ( $d_6$ -DMSO).

TABLE 1  
MOLECULAR WEIGHT OF JHDI/JTA EVALUATED FROM  $^1\text{H}$  NMR, MALDI-TOF MASS SPECTROSCOPY AND GPC

Sample	$^1\text{H}$ NMR <sup>a</sup>	Maldi-Tof mass spectroscopy <sup>b</sup>			GPC <sup>c</sup>		
	$M_n$ (g/mol)	$M_n$ (g/mol)	$M_w$ (g/mol)	PDI	$M_n$ (g/mol)	$M_w$ (g/mol)	PDI
JHDI	5009	5405	5545	1.03	6081	7175	1.18
JTA	8289	8952	9848	1.10	9445	11646	1.23

The resulting JTA is an elastomer with fracture strain ( $\epsilon_f$ ) of 813% at fracture stress ( $\sigma_f$ ) of 0.2MPa (Figure S1) and moreover, it is a healable elastomer with high healing efficiency. All these referred to the unique molecular feature of JTA that the soft PPO chains represent the stretchable part while the aromatic TA terminals provide the reversible aromatic  $\pi$ - $\pi$  and H bond interactions required for the mechanical strength and the observed autonomous recovery process. More importantly, the aromatic TA terminals of JTA can bind to MWCNT, rendering JCx composites with varied MWCNT contents (from 1 to 96 wt%).

### 3.1 Sorption isotherm and morphology

The superior mechanical and electrical behavior of MWCNT stimulated our study on using MWCNT as building block to develop advanced JCTx composites. Generally, transforming MWCNT into soluble materials that can be easily manipulated in the solution state may be subjected to dispersion difficulty and so, the effective utilization of MWCNT strongly depends on two factors: homogeneous dispersion of nanotubes throughout the polymer matrix without destroying the integrity of the tubes, and adequate interfacial adhesion between the nanotubes and polymers. The first factor can be demonstrated by the homogeneity of the solutions we prepared (Figure 2(a)), in which the dispersed MWCNTs can remained in the solution after a long period of time ( $> 1$  month), which demonstrated the great dispersion power of JTA for MWCNTs. The second factor can be seen from the elastomeric properties of certain elastomeric JCTx ( $x = 10$  to 40), which can sustain high strain (with high  $\epsilon_f$  values ranging from 100 to 700%) without mechanical failure.

Basically, there are four commonly used models<sup>56</sup> for nonlinear isotherm behavior, including Langmuir (LM), Dual-mode (DMM), Dual-Langmuir (DLM), and Freundlich (FM) models. Specially, the LM was developed to describe individual chemical adsorbents and is applicable to monolayer physical adsorption<sup>57</sup>, and DMM model was originally proposed for describing the sorption behavior of natural organic matters<sup>58</sup>. The FM is an empirical approach for adsorbents with uneven adsorbing site energy and is applicable to adsorption for a single-solute system within high- and middle-concentration environments. For FM, the goodness of fit varied with the MWCNTs (Figure S2a). The results suggested that the fit of FM is better than LM at high concentration but is worse at other range. Good fit was obtained for DLM (Figure S2b) with adj r2

0.98. However, two parameters among the four, i.e., adsorbed capacity ( $Q_2^0$ ) and DLM constant ( $b_2$ ) of site population 2 were significantly unreliable with  $p \gg 0.01$  (Table S1). Thus, the sorption process of JTA by MWCNTs may not be limited by the two types of adsorption sites. As a result<sup>50</sup>, our initial attempt for sorption used both DMM and LM to fit our experimental result.

The result from LM estimation deviated from the experimental data of JTA by MWCNTs (Figure S3), which can be also seen from the low adj  $r^2$  value of 0.87. Significant deviation of LM result from the experimental data was observed for LM at high concentration. The deviation indicates that the sorption of JTA, on the MWCNTs, may not be monolayer formation on a homogeneous surface, that is, the MWCNTs aggregated in the JTA solutions and the adsorbed JTA monolayer may continue to sorb the dissolved JTA molecules, via H bonds and other polar interactions, till the state that most MWCNT aggregates were surrounded by majority of JTA polymers.

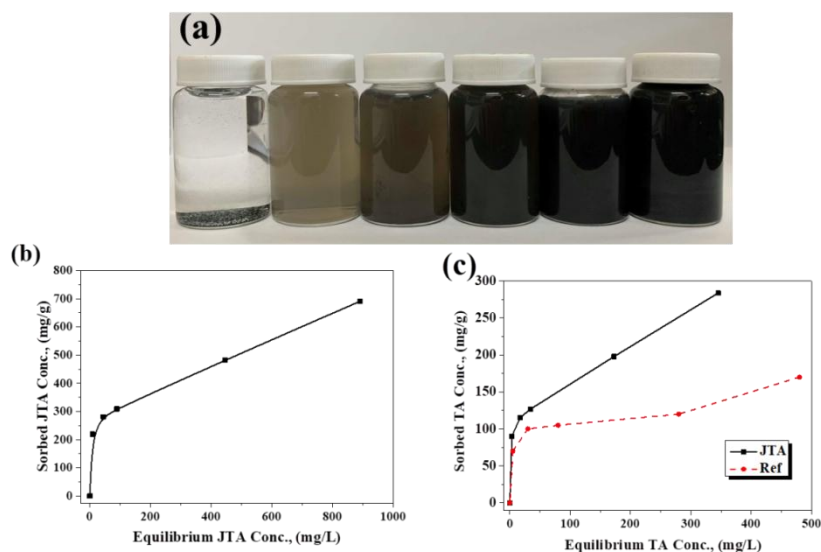


**FIGURE 2. (a) Solutions of MWCNT (200 mg/L) in DMF (20 mL) with varied concentrations of JTA (from left to right: with 0, 8.9, 44.5, 89, 445 and 890 mg of JTA in 1 L of DMF, respectively) (b) sorption isotherms of JTA and MWCNTs revealed a good fit with the theoretical curves predicted by the dual-mode model (DMM) and (c) compared with the result based on pure TA (dashed line) and MWCNT of the same dimensions.**

Sorption isotherms by DMM was examined in Figure 2(b), which exhibited non-linear relationship between equilibrium and sorbed JTA concentrations. We further transformed the JTA concentration into TA terminal concentration (Figure 2(c)) based on the  $^1\text{H}$  NMR result that  $M_n$  of JTA is 8289 g/mol and there are 1.89 TA terminals per JTA chain. Both non-linear isotherms in Figure 2(b) and 2(c), using parameters (Table S1) of MWCNT with the respective inner and outer diameters of 10 and 20 nm, revealed a good fit between DMM estimation<sup>58</sup> and experimental results. The good fits (adj  $r^2$  is 0.99) suggested that the sorption of JTA by MWCNT followed the same two-step sorption model previously proposed for pure TA on MWCNTs<sup>50</sup> that TA terminals of JTA may be sorbed first onto MWCNTs with its aromatic rings binding to the surface carbon rings of MWCNT via  $\pi$ - $\pi$  interactions, until forming a monolayer, and then the JTA monolayer formed further sorbed the dissolved JTA by H bonds and other polar interactions. The sorbed JTA increased the steric repulsion between individual MWCNTs, which might disperse the relatively loose MWCNT aggregates and result in the stabilization of MWCNTs in JTA solution.

Experimental data in Figure 2(c) also compared with the result<sup>50</sup> from pure TA (dashed line) and MWCNT of the same dimensions. Despite being lower in TA concentration, JTA nevertheless is superior to pure TA in dispersing MWCNTs. We attributed this high dispersion power of JTA to two factors: DMF solvent used in our example is a better dispersion solvent for MWCNTs than water used in previous case. Moreover, with the PPO chain, JTA should be superior to TA in hydrophobicity and in dispersing the hydrophobic MWCNTs. The superior dispersion power of JTA thereby imparts high loads of MWCNTs in DMF, providing JCTx composites containing large amounts of MWCNTs (from 10 to 96 wt%) after removal of DMF.

The solid JCTx composites are either stretchable elastomers when  $x \leq 40$  (Table 2) or rigid and highly conductive plastics when  $x > 50$ . The morphology of JCTx with small (40 wt%, Figure 3(a)), medium (70 wt%, Figure 3(b)) and large (96 wt%, Figure 3(c)) concentrations of MWCNTs was primarily examined by SEM. The resolved images are fundamentally similar with each other, all exhibiting tree branch-like bunches in micrometer sizes all over the samples. The randomly distributed branches should consist of inner MWCNT core wrapped by outer JCTx wall. The higher is the MWCNT content; the lower is the diameter of the resolved branches. The branches with smaller diameter may have tighter aggregation and entanglement, which may not be able to be dispersed by JTA during the preparation step in DMF. The looser agglomerates of the larger branches could be dispersed by JTA with shaking in DMF. The branch density also increased with increasing MWCNT content and the highest MWCNT-loaded JCT96 composite exhibited a morphology that the densely packed branches were interconnected with each other to result in a 3D crosslinked network with irregular, large knots, constituted by aggregated and entangled MWCNTs, as the crosslinking points to maintain the integrity of JCT96.

**TABLE 2**  
**CHARACTERISTICS OF THE JTA COMPOSITES FROM JCT1 TO JCT96**

	Mass fraction $p$ (%)	Volume fraction $\phi_f$ (%)	Density (g/ml)	Stretchability ( $\epsilon_\phi$ MPa, $\sigma_f$ %)	Conductivity $\sigma$ (S.m <sup>-1</sup> )
JTA	----	-----	1.17	Yes ( 813, 0.20 )	----- <sup>-3</sup>
JCT1	1	0.01	1.18	Yes ( 797, 0.23 )	$1.2 \times 10^{-2}$
JCT10	10	0.09	1.20	Yes ( 690, 0.52 )	$7.14 \times 10^{-1}$
JCT20	20	0.18	1.24	Yes ( 524, 0.80 )	$9.84 \times 10^1$
JCT30	30	0.26	1.27	Yes ( 350, 3.09 )	$3.2 \times 10^2$
JCT40	40	0.32	1.30	Yes ( 175, 6.06 )	$6.55 \times 10^3$
JCT50	50	0.41	1.34	No (--)	$3.02 \times 10^3$
JCT60	60	0.49	1.37	No (--)	$9.15 \times 10^3$
JCT70	70	0.59	1.40	No (--)	$6.76 \times 10^4$
JCT80	80	0.70	1.43	No (--)	$3.46 \times 10^5$
JCT90	90	0.84	1.47	No (--)	$8.31 \times 10^5$
JCT96	96	0.92	1.49	No (--)	$1.21 \times 10^6$

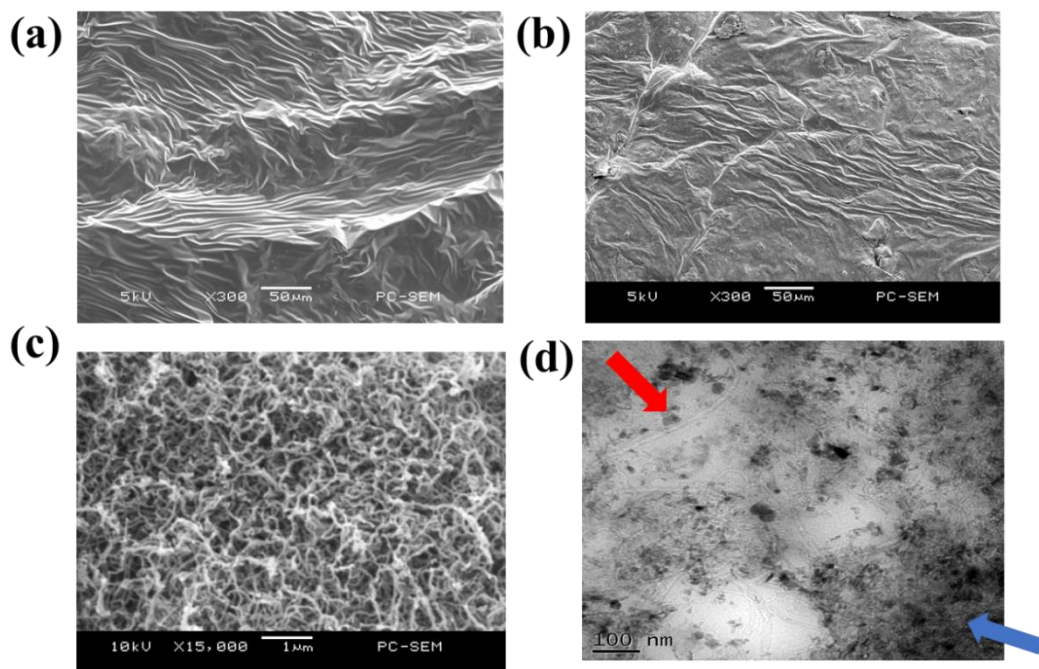


**FIGURE 3. SEM images of (a) JCT40, (b) JCT70, and (c) JCT96 and TEM image of (d) JCT50**

To see the interior of the tree branch, a JCT50 sample was then investigated by TEM. The small, white spherical images of the TEM micrograph (Figure 3(d)), which illustrated the vertical view of MWCNTs, are due to the inner empty core while the black images in between the white ones represent the outer wall of MWCNT. All these vertically erected MWCNTs are aggregated into large bundles and interestingly, all these vertical bundles are surrounded by extended rope-shaped tubes (red arrow), which represent the parallel view of MWCNT with the respective inner and outer diameters of 9.6 and 18.8 nm, close to the respective values of 10 and 20 nm given by the supplier. The sharp boundary between the inner vertical bundle and the outer parallel tube corresponds to flaws with mechanical weakness, which should lower the mechanical strength of the JCTx composites, a point will be discussed next. It is difficult to avoid aggregation of MWCNTs into bundle in considering that the TA terminals of JTA are insufficient in number to cover all the vast surfaces of the nano-sized MWCNTs. In consequence, a plethora of MWCNTs should associate together into large-sized bundles with much reduced surface areas to be covered by JTAs. Besides the MWCNT bundles, there are certain large black regions, which should correlate with the embedded JTA aggregates and the JTA polymer in the interphase region (blue arrow). Several vertical MWCNT bundles inside the interphase region may be an indication of how well the MWCNTs can be dispersed by JTA.

### 3.2 Mechanical properties of the JCTx composite films.

As the effective conductor, MWCNT also acted to reinforce the mechanical strength of the JCTx composites. Without MWCNT, pure JTA is soft and highly stretchable with the resolved  $\epsilon_f$  value of 813% (Figure 4(a)) and the incorporation of rigid MWCNTs raised the mechanical strength at the expense of stretchability of the JCTx ( $x \leq 40$ ) films. With 40 wt% of rigid MWCNT, the JCT40 composite is still an elastomer with a high  $\epsilon_f$  value of near 200% (Table 2), which demonstrated the strong interfacial adhesion between MWCNT and JTA. Higher content of rigid MWCNT nevertheless resulted in non-stretchable, rigid JCTx ( $x \geq 40$ ) composites. Because all the JCTx composites prepared in this study having a MWCNT content well beyond the percolation threshold (generally,  $< 0.1$  wt%), the mechanical and conductive characterizations conducted hereafter are unprecedented.

Because the SEM image of JCT40 (Figure 3(a)) suggested the continuous distribution of the branches over the polymer matrices, the Kolarik<sup>54</sup> model based on a 3D cross-orthogonal skeleton (COS) should be appropriate in analyzing the mechanical property of the stretchable JCTx ( $x$  from 0 to 40 wt%) at concentration well above the percolation threshold. Based on the COS structure, Kolarik calculated the tensile modulus ( $E$ ) of the composites with co-continuous morphology using:

$$E = E_m(1 - f^2) + E_f f^2 + [f(1-f) E_m] / [1 - f + (f E_m / E_f)] \quad (1)$$

$$1 - \Phi_f - (1-f)^2(1+2f) = 0 \quad (2)$$

Where in equation (1),  $E_f$  and  $E_m$  are the tensile moduli of the filler and the JTA polymer matrix, respectively,  $\Phi_f$  is the filler volume fraction and the  $\Phi_f$ -dependent parameter  $f$  can be determined from equation (2). Rather than small nanotubes, the filler phase contained in JCTx are large branches constituted by rigid MWCNT bundle core surrounded by soft JTA walls, which also is correlated with a 3D co-continuous structure and should be valid for Kolarik approach, too.

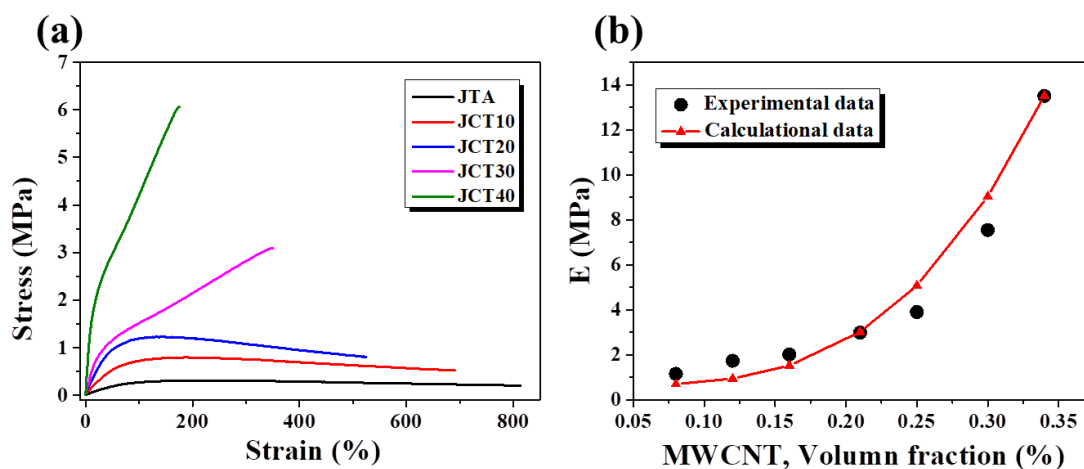


FIGURE 4. (a) Stress-strain curves and (b) comparison of the experimental moduli  $E_s$  of JCTx ( $x$  from 10 to 40) with the theoretical values determined from equation (1)

The experimental E values as function of MWCNT content were plotted in Figure 4(b) to correlate with the calculated results based on Kolarik model. The  $E_m$ ,  $E_f$  and parameter  $f$  involved in calculation of the theoretical E values were summarized in Table S2. The results depicted in Figure 4(b) clearly indicated the fair agreement between the experimental and the theoretical data. The  $E_f$  value of 85.6 MPa was obtained from fitting experimental E value of JCT40 into equation (1). Previous approach had commented on the dilemma in evaluating the mechanical property of MWCNT: although the strength of individual CNT shells is extremely high (with E up to 1,000 GPa), weak shear interactions between adjacent shells and tubes lead to significant reduction<sup>59</sup> in the effective strength of MWCNTs and CNT bundles down to few GPa. The present case nevertheless illustrated an even lower  $E_f$  value of 85.6 MPa, which may be attributed to the nature of the structural unit evaluated from SEM and TEM analysis. Instead of MWCNT bundles, the responsive structural unit in JCTx is branches consisting of inner MWCNT bundles wrapped by the outer polymer wall. The embedded polymer and the polymer wall all are soft segments representative of mechanical weak points acting to lower the E value of the JCTx composites, which is plausible for the low  $E_f$  value of 85.6 MPa for JCT40.

### 3.3 Conductive properties of the JCTx composite films.

JTA polymer is an insulator but the incorporation of MWCNT with a concentration well beyond percolation threshold resulted in conductive composite with high conductivity (Table 2). At percolation threshold, conducting network forms in the polymer matrix starts to transfer electrons and creates the conductivity. SEM images (Figure 3(a) ~ (c)) revealed the presence of branches, which constituted the interconnected network effective in transferring electrons, in the JCTx composites. All JCTx composites are good at electron transfer according to the result that JCT1 is a semi-conductor with a conductivity of  $1.2 \times 10^{-3} \text{ Sm}^{-1}$ , and the increase of MWCNT content enhanced the conductivity to an ultimate high value of  $1.21 \times 10^6 \text{ S m}^{-3}$  for JCT96. Essentially, the dense-packed branches of JCT96 contributed to its high conductivity, which is close to the conductivity ( $10^7 \text{ Sm}^{-1}$ ) of pure MWCNT.

According to classical percolation theory<sup>55</sup>, the conductivity of composite materials as conductive filler content is increased can be described by a scaling law of the form

$$\sigma \propto (\pi - \pi_c)^t \quad (3)$$

where  $\sigma$  is conductivity,  $p$  is mass fraction,  $p_c$  is the electric percolation threshold (EPT)<sup>55</sup> and exponent  $t$  is expected to depend on sample dimensionality with calculated values of  $\sim 1.33$  and  $\sim 2.0$  in 2 D and 3 D arrangements, respectively. For the present case,  $p$  is much larger than  $p_c$ , therefore eqn (3) can be further simplified:

$$\sigma \propto p^t \quad (4)$$

In Figure 5(a), the dc conductivity data are shown on a semilogarithmic scale versus  $\ln(p)$ . The expected linear relationship is observed, with the solid line as a good fit with a slope of 1.92. The resulting  $t$  value of 1.92 for JCTx is found to agree with the universal value of 2 observed for composites in which the conductive fillers form a continuous 3D percolating path throughout the matrix<sup>60</sup>. The percolation path of JCTx refers to the continuous branches distributed randomly in 3D dimension.

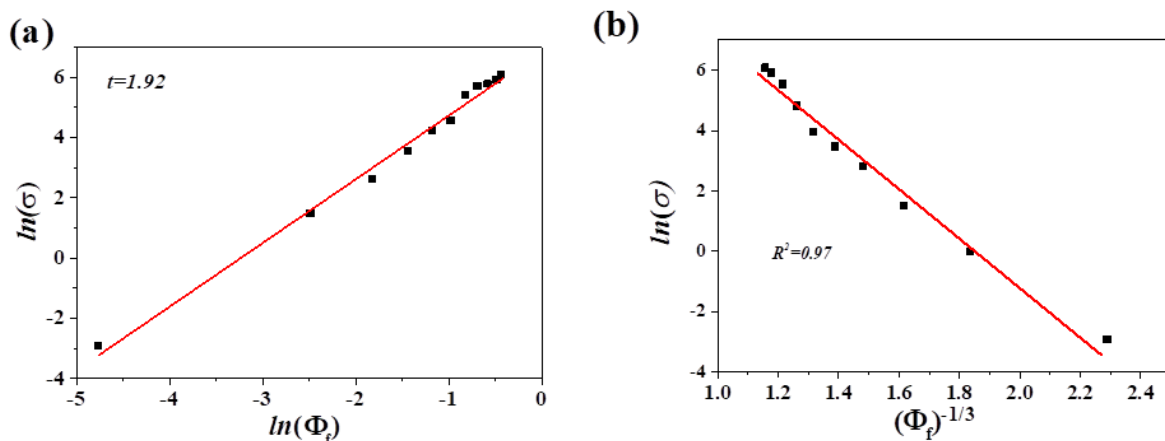


FIGURE 5. Comparison of experimental conductivity of JCTx (x from 10 to 96) with the theoretical values determined from the scaling law of (a) eqn (4) and (b) eqn (5)

The change in the electrical conductivity of the composite materials, when the EPT is reached in coincidence with the formation of a conductive path inside the material, can be interpreted in terms of electron tunneling. According to this model the electrons “jump” from a conductor to the closest stone over a small distance of the order of a few nanometers<sup>61</sup>. A method reported in literature<sup>62,63,55</sup> to verify that the electron tunneling is the main electrical transport mechanism in nano filled resins is based on the occurrence of a linear relation (Fig. 5(b)) between the electrical conductivity (in natural logarithmic scale) and  $p^{-1/3}$ , valid for mass fraction ( $p$ ) above EPT:

$$\ln(\sigma) \propto p^{-1/3} \quad (5)$$

The straight line is the fit curve of the experimental data: the value of  $R^2$  here is close to 1, which confirms that the electrical conduction network in the composite materials is mainly achieved through the quantum tunneling effect. The current and therefore the electrical conductivity of the resulting composites are related to the intrinsic features of the adopted conductive filler. The conductive filler illustrates here covered the whole branch consisting of MWCNT core and JTA wall, which provides 3D conductive paths for fluent transport of electrons. The TEM and SEM images (Figure 3) suggested the presence of several conductive flaws, including boundary between the vertical MWCNT bundles and the surrounding parallel tubes, the interfacial region and the polymer insulator between branches, in the composites. At these conductive flaws, electrons had to “jump” from one MWCNT to the closest stone over a small distance of a few nanometers, resulting in the perfect fit of experimental data to equation (5).

#### IV. CONCLUSION

Through deliberate molecular engineering, we synthesized a TA-terminated JTA polymer with inherent aromatic phenolic rings and hydroxyl OH groups to promote the desired elasticity. The aromatic phenolic rings of JTA also bind to the surface carbon rings of MWCNTs, thus generating homogeneous JCTx composites with low (e.g. 10 wt%) and high (96 wt%) MWCNT contents.

Tree branches, constituted by inner MWCNT bundles and outer JTA walls, are interconnected with each other to form a 3 D crosslinked network of JCTx composites. With concentration well above percolation threshold, soft JCTx (x from 1 to 40 wt%) exhibited the elastic modulus correlated with theoretical Kolarix model based on All JCTx (x from 1 to 96) composites are conductive materials and the increase of MWCNT content largely promoted the composite conductivity to an ultimate excellent value of  $1.2 \times 10^6 \text{ S m}^{-1}$  for the JCT96. The conductivity of the JCTx composites can be appropriately fitted by the scaling law of  $\sigma \propto \rho^{-1.92}$  according to a 3D network model. The tree branches are responsible for the effective electron transfer and the ideal conductivity behaviors of the JCTx samples.

Dependent on the MWCNT content, the JCTx composite sensors can be highly stretchable or highly conductive. The highly conductive JCT96 is a sensitive sensor with keen response toward minor pulse beating. With good stretchability, the soft JCT40 is a stable sensor for the steady detection of large elbow bending motion. With the lowest MWCNT content, JCT10 is capable of repeatedly detecting a high strain of 220%. Through manipulating composite composition, JCTx sensors with the desired mechanical and conductive properties can be conveniently prepared and characterized. The developed JCTx composites in this study can also be applied to other practical application fields such as supercapacitor or lithium ion battery.

#### ACKNOWLEDGEMENTS

We appreciate the financial support from Ministry of Science and Technology (MOST), ROC, under the contract MOST 108-2221-E-110-015.

#### REFERENCES

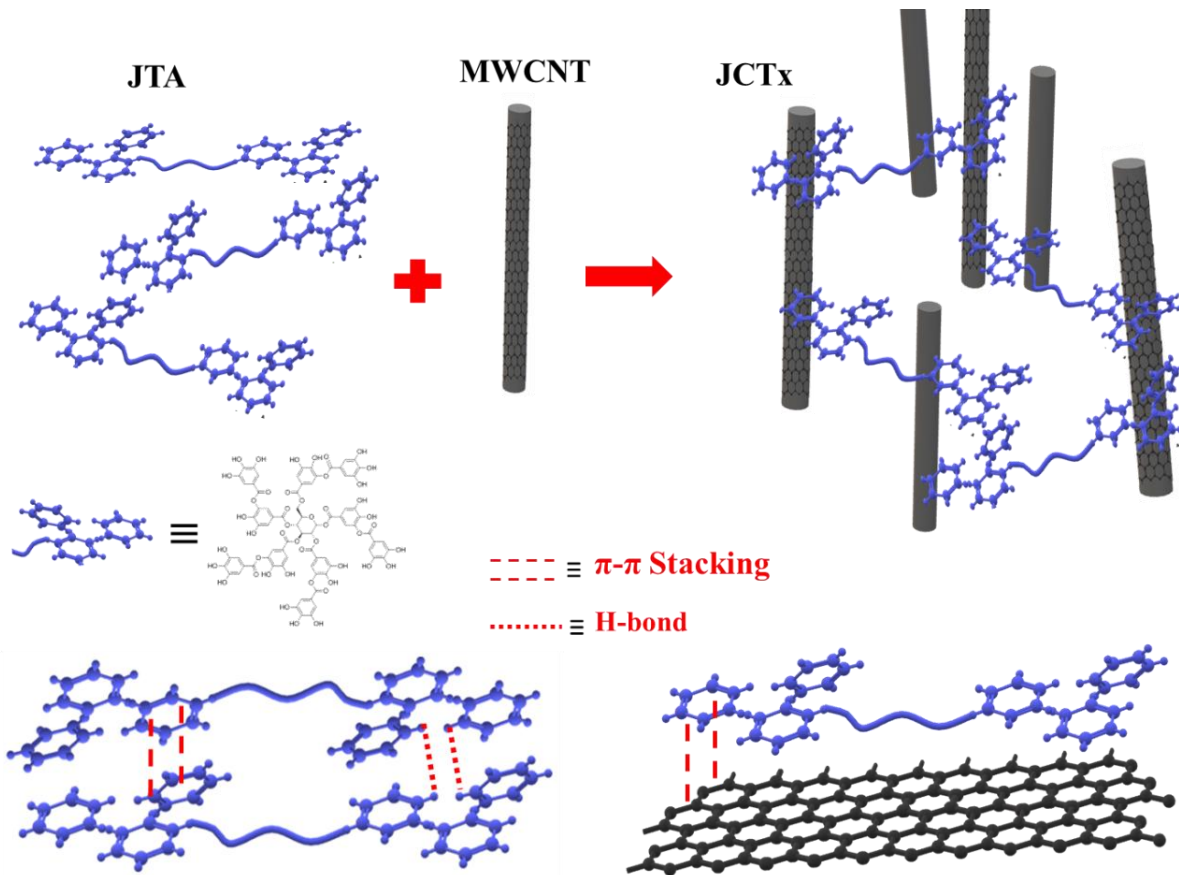
- [1] Ajayan, P. M., Nanotubes from carbon. Chemical reviews 1999, 99, 1787-1800.
- [2] Dresselhaus, G.; Riichiro, S., Physical properties of carbon nanotubes. World scientific: 1998.
- [3] Barraza, H. J.; Pompeo, F.; O'Rea, E. A.; Resasco, D. E., SWNT-filled thermoplastic and elastomeric composites prepared by miniemulsion polymerization. Nano letters 2002, 2, 797-802.
- [4] Du, F.; Fischer, J. E.; Winey, K. I., Coagulation method for preparing single-walled carbon nanotube/poly (methyl methacrylate) composites and their modulus, electrical conductivity, and thermal stability. Journal of Polymer Science Part B: Polymer Physics 2003, 41, 3333-3338.
- [5] Probst, O.; Moore, E. M.; Resasco, D. E.; Grady, B. P., Nucleation of polyvinyl alcohol crystallization by single-walled carbon nanotubes. Polymer 2004, 45, 4437-4443.
- [6] Hertel, T.; Walkup, R. E.; Avouris, P., Deformation of carbon nanotubes by surface van der Waals forces. Physical review B 1998, 58, 13870.

- [7] Heintz, A. M.; Risser, S. M.; Moore, B. P.; Elhard, J. D.; Cucksey, C. M., Carbon nanotube films and methods of forming films of carbon nanotubes by dispersing in a superacid. Google Patents: 2019.
- [8] Huang, Y. Y.; Terentjev, E. M., Dispersion of carbon nanotubes: mixing, sonication, stabilization, and composite properties. *Polymers* 2012, 4, 275-295.
- [9] Liang, Y.; Hilal, N.; Langston, P.; Starov, V., Interaction forces between colloidal particles in liquid: Theory and experiment. *Advances in colloid and interface science* 2007, 134, 151-166.
- [10] Israelachvili, J. N., Intermolecular and surface forces. Academic press: 2011.
- [11] Huang, J.-E.; Li, X.-H.; Xu, J.-C.; Li, H.-L., Well-dispersed single-walled carbon nanotube/polyaniline composite films. *Carbon* 2003, 41, 2731-2736.
- [12] Ma, P.-C.; Siddiqui, N. A.; Marom, G.; Kim, J.-K., Dispersion and functionalization of carbon nanotubes for polymer-based nanocomposites: a review. *Composites Part A: Applied Science and Manufacturing* 2010, 41, 1345-1367.
- [13] Qian, H.; Greenhalgh, E. S.; Shaffer, M. S.; Bismarck, A., Carbon nanotube-based hierarchical composites: a review. *J Mater Chem* 2010, 20, 4751-4762.
- [14] McLachlan, D.; Heaney, M. B., Complex ac conductivity of a carbon black composite as a function of frequency, composition, and temperature. *Physical Review B* 1999, 60, 12746.
- [15] Lafosse, X., Percolation and dielectric relaxation in polypyrrole-Teflon alloys. *Synthetic metals* 1995, 68, 227-231.
- [16] Ramdeen, F.; Hill, R., Scaling in the Region of the Percolation Threshold. *physica status solidi (b)* 1999, 213, 391-395.
- [17] Cai, W.; Li, M.; Wang, S.; Gu, Y.; Li, Q.; Zhang, Z., Strong, flexible and thermal-resistant CNT/polyarylacetylene nanocomposite films. *Rsc Adv* 2016, 6, 4077-4084.
- [18] Wu, T.; Chen, B., Autonomous self-healing multiwalled carbon nanotube nanocomposites with piezoresistive effect. *Rsc Adv* 2017, 7, 20422-20429.
- [19] Tsonos, C.; Soin, N.; Tomara, G.; Yang, B.; Psarras, G. C.; Kanapitsas, A.; Siores, E., Electromagnetic wave absorption properties of ternary poly (vinylidene fluoride)/magnetite nanocomposites with carbon nanotubes and graphene. *Rsc Adv* 2016, 6, 1919-1924.
- [20] Kaur, T.; Thirugnanam, A., Tailoring in vitro biological and mechanical properties of polyvinyl alcohol reinforced with threshold carbon nanotube concentration for improved cellular response. *Rsc Adv* 2016, 6, 39982-39992.
- [21] Marroquin, J. B.; Rhee, K.; Park, S., Chitosan nanocomposite films: enhanced electrical conductivity, thermal stability, and mechanical properties. *Carbohydrate polymers* 2013, 92, 1783-1791.
- [22] Tzounis, L.; Liebscher, M.; Tzounis, A.; Petinakis, E.; Paipetis, A.; Mäder, E.; Stamm, M., CNT-grafted glass fibers as a smart tool for epoxy cure monitoring, UV-sensing and thermal energy harvesting in model composites. *Rsc Adv* 2016, 6, 55514-55525.
- [23] Rostami, A.; Nazockdast, H.; Karimi, M., Graphene induced microstructural changes of PLA/MWCNT biodegradable nanocomposites: rheological, morphological, thermal and electrical properties. *Rsc Adv* 2016, 6, 49747-49759.
- [24] Zare, Y.; Garmabi, H.; Rhee, K. Y., Structural and phase separation characterization of poly (lactic acid)/poly (ethylene oxide)/carbon nanotube nanocomposites by rheological examinations. *Composites Part B: Engineering* 2018, 144, 1-10.
- [25] Zare, Y.; Rhee, K. Y., Prediction of tensile modulus in polymer nanocomposites containing carbon nanotubes (CNT) above percolation threshold by modification of conventional model. *Current Applied Physics* 2017, 17, 873-879.
- [26] Zhu, J.-M.; Zare, Y.; Rhee, K. Y., Analysis of the roles of interphase, waviness and agglomeration of CNT in the electrical conductivity and tensile modulus of polymer/CNT nanocomposites by theoretical approaches. *Colloids and Surfaces A: Physicochemical and Engineering Aspects* 2018, 539, 29-36.
- [27] Al-Saleh, M. H., Influence of conductive network structure on the EMI shielding and electrical percolation of carbon nanotube/polymer nanocomposites. *Synthetic Metals* 2015, 205, 78-84.
- [28] Logakis, E.; Pissis, P.; Pospiech, D.; Korwitz, A.; Krause, B.; Reuter, U.; Pötschke, P., Low electrical percolation threshold in poly (ethylene terephthalate)/multi-walled carbon nanotube nanocomposites. *Eur Polym J* 2010, 46, 928-936.
- [29] Li, H.-x.; Zare, Y.; Rhee, K. Y., The percolation threshold for tensile strength of polymer/CNT nanocomposites assuming filler network and interphase regions. *Materials Chemistry and Physics* 2018, 207, 76-83.
- [30] Razavi, R.; Zare, Y.; Rhee, K. Y., A model for tensile strength of polymer/carbon nanotubes nanocomposites assuming the percolation of interphase regions. *Colloids and Surfaces A: Physicochemical and Engineering Aspects* 2018, 538, 148-154.
- [31] Martin-Gallego, M.; Bernal, M.; Hernandez, M.; Verdejo, R.; López-Manchado, M. A., Comparison of filler percolation and mechanical properties in graphene and carbon nanotubes filled epoxy nanocomposites. *Eur Polym J* 2013, 49, 1347-1353.
- [32] Zare, Y.; Rhee, K. Y., Development of a conventional model to predict the electrical conductivity of polymer/carbon nanotubes nanocomposites by interphase, waviness and contact effects. *Composites Part A: Applied Science and Manufacturing* 2017, 100, 305-312.
- [33] Zare, Y.; Rhee, K. Y., Development of a model for electrical conductivity of polymer/graphene nanocomposites assuming interphase and tunneling regions in conductive networks. *Industrial & Engineering Chemistry Research* 2017, 56, 9107-9115.
- [34] Zare, Y.; Rhee, K. Y., Development and modification of conventional Ouali model for tensile modulus of polymer/carbon nanotubes nanocomposites assuming the roles of dispersed and networked nanoparticles and surrounding interphases. *Journal of colloid and interface science* 2017, 506, 283-290.
- [35] Almagableh, A.; Mantena, R.; Alostaz, A.; Rababah, M.; Aljarrah, M.; Awad, A. S., Modeling the elastic modulus of exfoliated graphite platelets filled vinyl ester: analytical predictions with consideration of filler percolation. *Journal of Composite Materials* 2015, 49, 1285-1290.

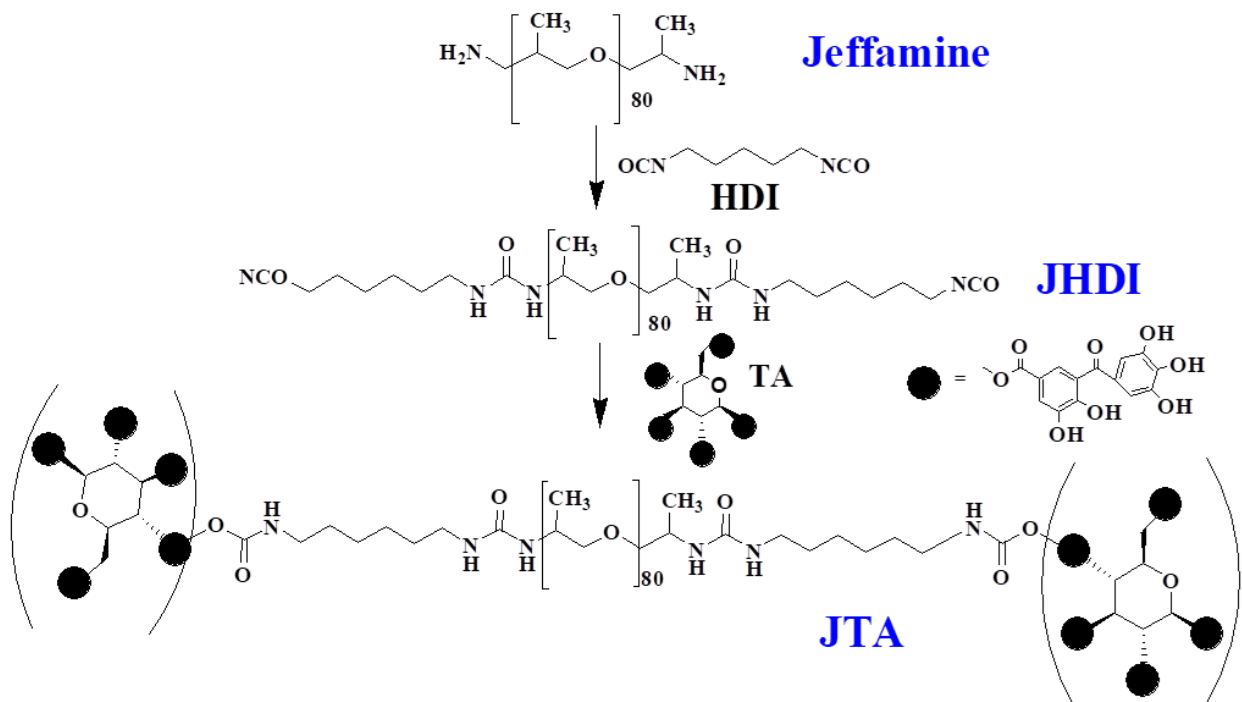
- [36] Kim, J. Y.; Park, H. S.; Kim, S. H., Multiwall-carbon-nanotube-reinforced poly (ethylene terephthalate) nanocomposites by melt compounding. *Journal of applied polymer science* 2007, 103, 1450-1457.
- [37] Heller, D. A.; Barone, P. W.; Swanson, J. P.; Mayrhofer, R. M.; Strano, M. S., Using Raman spectroscopy to elucidate the aggregation state of single-walled carbon nanotubes. *The Journal of Physical Chemistry B* 2004, 108, 6905-6909.
- [38] Bergman, S. D.; Wudl, F., Mendable polymers. *J Mater Chem* 2008, 18, 41-62.
- [39] Du, P.; Wu, M.; Liu, X.; Zheng, Z.; Wang, X.; Sun, P.; Joncheray, T.; Zhang, Y., Synthesis of linear polyurethane bearing pendant furan and cross-linked healable polyurethane containing Diels–Alder bonds. *New Journal of Chemistry* 2014, 38, 770-776.
- [40] Thostenson, E. T.; Chou, T. W., Carbon nanotube networks: Sensing of distributed strain and damage for life prediction and self healing. *Adv Mater* 2006, 18, 2837-3841.
- [41] Tee, B. C.; Wang, C.; Allen, R.; Bao, Z., An electrically and mechanically self-healing composite with pressure- and flexion-sensitive properties for electronic skin applications. *Nat Nanotechnol* 2012, 7, 825-832.
- [42] Benight, S. J.; Wang, C.; Tok, J. B. H.; Bao, Z. A., Stretchable and self-healing polymers and devices for electronic skin. *Prog Polym Sci* 2013, 38, 1961-1977.
- [43] Gao, Y.; Fang, X.; Tan, J.; Lu, T.; Pan, L.; Xuan, F., Highly sensitive strain sensors based on fragmented carbon nanotube/polydimethylsiloxane composites. *Nanotechnology* 2018, 29, 235501.
- [44] Yang, H.; Yao, X.; Yuan, L.; Gong, L.; Liu, Y., Strain-sensitive electrical conductivity of carbon nanotube-graphene-filled rubber composites under cyclic loading. *Nanoscale* 2019, 11, 578-586.
- [45] Cai, L.; Song, L.; Luan, P.; Zhang, Q.; Zhang, N.; Gao, Q.; Zhao, D.; Zhang, X.; Tu, M.; Yang, F.; Zhou, W.; Fan, Q.; Luo, J.; Zhou, W.; Ajayan, P. M.; Xie, S., Super-stretchable, transparent carbon nanotube-based capacitive strain sensors for human motion detection. *Sci Rep* 2013, 3, 3048.
- [46] Zhao, S. F.; Li, J. H.; Cao, D. X.; Gao, Y. J.; Huang, W. P.; Zhang, G. P.; Sun, R.; Wong, C. P., Percolation threshold-inspired design of hierarchical multiscale hybrid architectures based on carbon nanotubes and silver nanoparticles for stretchable and printable electronics. *Journal of Materials Chemistry C* 2016, 4, 6666-6674.
- [47] Mai, H.; Mutlu, R.; Tawk, C.; Alici, G.; Sencadas, V., Ultra-stretchable MWCNT–Ecoflex piezoresistive sensors for human motion detection applications. *Composites Science and Technology* 2019, 173, 118-124.
- [48] Liu, H.; Li, Y.; Dai, K.; Zheng, G.; Liu, C.; Shen, C.; Yan, X.; Guo, J.; Guo, Z., Electrically conductive thermoplastic elastomer nanocomposites at ultralow graphene loading levels for strain sensor applications. *Journal of Materials Chemistry C* 2016, 4, 157-166.
- [49] Liu, W. C.; Chung, C. H.; Hong, J. L., Highly Stretchable, Self-Healable Elastomers from Hydrogen-Bonded Interpolymer Complex (HIPC) and Their Use as Sensitive, Stable Electric Skin. *Acs Omega* 2018, 3, 11368-11382.
- [50] Lin, D.; Xing, B., Tannic acid adsorption and its role for stabilizing carbon nanotube suspensions. *Environ Sci Technol* 2008, 42, 5917-5923.
- [51] Zhang, X.; Liu, M.; Zhang, X.; Deng, F.; Zhou, C.; Hui, J.; Liu, W.; Wei, Y., Interaction of tannic acid with carbon nanotubes: enhancement of dispersibility and biocompatibility. *Toxicology Research* 2015, 4, 160-168.
- [52] San Biagio, P.; Bulone, D.; Emanuele, A.; Palma, M., Self-assembly of biopolymeric structures below the threshold of random cross-link percolation. *Biophysical journal* 1996, 70, 494-499.
- [53] Ezquerra, T. A.; Kuleszcza, M.; Cruz, C. S.; Baltá-Calleja, F. J., Charge transport in polyethylene–graphite composite materials. *Adv Mater* 1990, 2, 597-600.
- [54] Chen, S.; Sarafbidabad, M.; Zare, Y.; Rhee, K. Y., Estimation of the tensile modulus of polymer carbon nanotube nanocomposites containing filler networks and interphase regions by development of the Kolarik model. *Rsc Adv* 2018, 8, 23825-23834.
- [55] Kilbride, B. e.; Coleman, J.; Fraysse, J.; Fournet, P.; Cadek, M.; Drury, A.; Hutzler, S.; Roth, S.; Blau, W., Experimental observation of scaling laws for alternating current and direct current conductivity in polymer-carbon nanotube composite thin films. *Journal of applied physics* 2002, 92, 4024-4030.
- [56] Chen, X., Modeling of experimental adsorption isotherm data. *Information* 2015, 6, 14-22.
- [57] Chang, M.-Y.; Juang, R.-S., Adsorption of tannic acid, humic acid, and dyes from water using the composite of chitosan and activated clay. *Journal of Colloid and Interface Science* 2004, 278, 18-25.
- [58] Xing, B.; Pignatello, J. J., Dual-mode sorption of low-polarity compounds in glassy poly (vinyl chloride) and soil organic matter. *Environ Sci Technol* 1997, 31, 792-799.
- [59] Filletter, T.; Bernal, R.; Li, S.; Espinosa, H. D., Ultrahigh strength and stiffness in cross-linked hierarchical carbon nanotube bundles. *Adv Mater* 2011, 23, 2855-2860.
- [60] Nan, C.-W.; Shen, Y.; Ma, J., Physical properties of composites near percolation. *Annual Review of Materials Research* 2010, 40, 131-151.
- [61] De Vivo, B.; Lamberti, P.; Spinelli, G.; Tucci, V., A morphological and structural approach to evaluate the electromagnetic performances of composites based on random networks of carbon nanotubes. *Journal of Applied Physics* 2014, 115, 154311.
- [62] Connor, M. T.; Roy, S.; Ezquerra, T. A.; Calleja, F. J. B., Broadband ac conductivity of conductor-polymer composites. *Physical Review B* 1998, 57, 2286.
- [63] Mdarhri, A.; Carmona, F.; Brosseau, C.; Delhaes, P., Direct current electrical and microwave properties of polymer-multiwalled carbon nanotubes composites. *Journal of applied physics* 2008, 103, 054303.

ANNEXURE: SUPPORTING INFORMATION

1) Scheme



SCHEME 1. The complexation of JTA and MWCNT to form JCTx composites and the potential interactions between JTA and MWCNT.



SCHEME 2. Synthesis of JHDI precursor and TA-terminated JTA

2) Supplementary Figures:

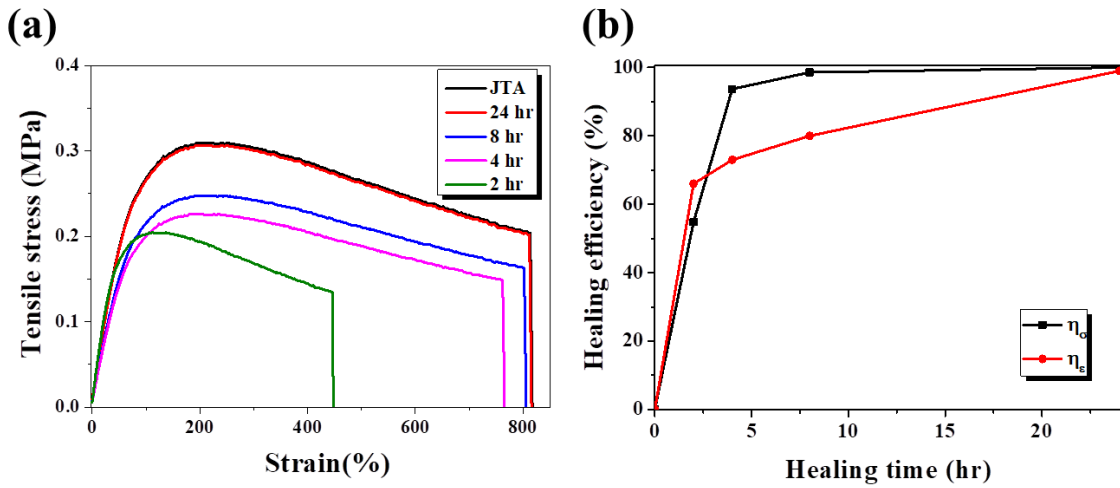


FIGURE S1. (a) Stress-strain curves and (b) the stress  $\eta_{\sigma}$  and strain  $\eta_{\epsilon}$  healing efficiencies of the pristine and the healed JTA after different time of autonomous recovery.

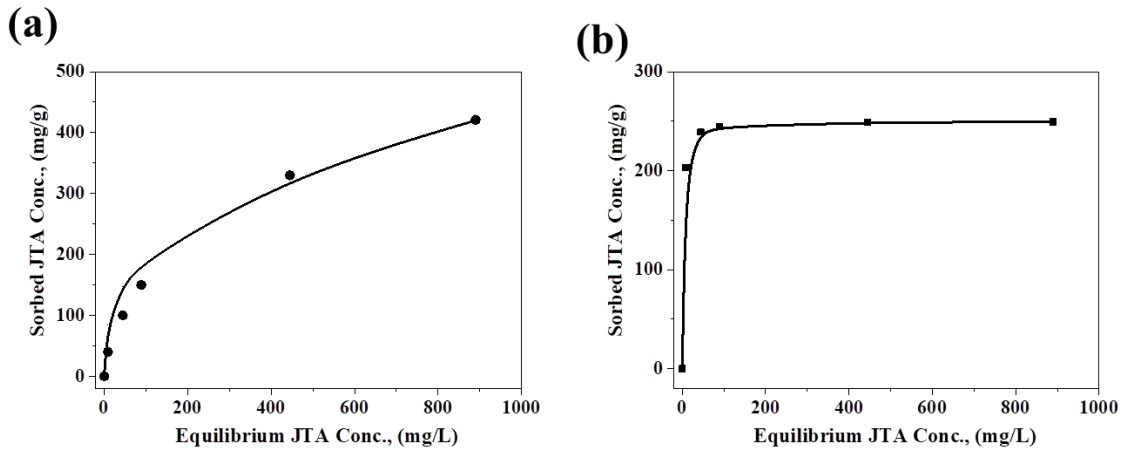


FIGURE S2. Model fits to the sorption data of JTA by carbon nanotubes (CNTs) by (a) Freundlich (FM) and (b) Dual-Langmuir (DLM) models.

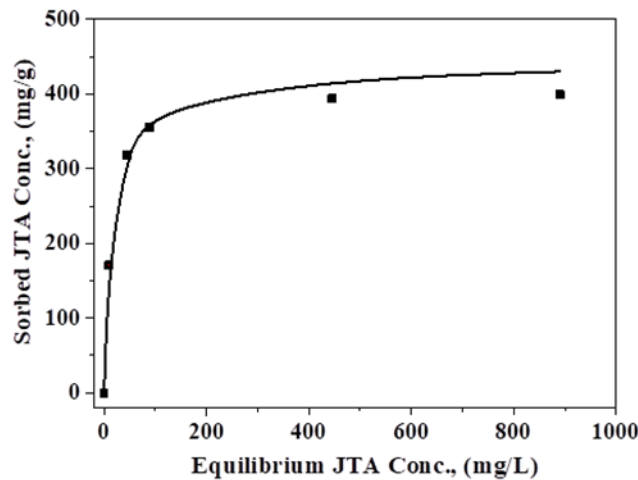


FIGURE S3. Model fits to the sorption data of JTA by carbon nanotubes (CNTs) by Langmuir model (LM).

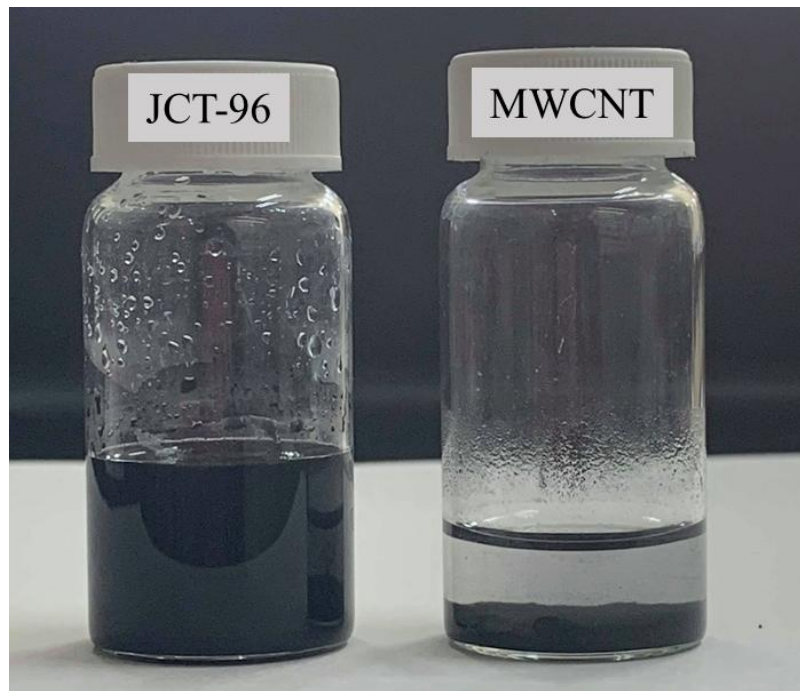


FIGURE S4. (a) Photo of JCT96/DMF (96 mg MWCNT/4 mg JTA /2 mL, left) MWCNT/DMF (100 mg/2 mL, right) solutions after settling for 30 days.

3) Supplementary Tables:

TABLE S1

MODEL EQUATION AND PARAMETER DEFINITION FITS TO SORPTION DATA

Langmuir model	$q_e = Q^0 b C_e / (1 + b C_e)$							
CNT	$Q^0$	p of $Q^0$	b	p of b				
MWCNT20	166	< 0.01	0.082	0.015				
Freundlich model	$q_e = K_f C_e^{1/n}$							
CNT	$K_f$	p of $K_f$	n	p of N				
MWCNT20	39	< 0.01	2.840	< 0.01				
Dual-model model	$q_e = Q^0 b C_e / (1 + b C_e) + K_d C_e$							
CNT	$Q^0$	p of $Q^0$	b	p of b	$K_d$	p of $K_d$		
MWCNT20	105	< 0.01	0.405	< 0.01	0.205	< 0.01		
Dual-langmuir model	$q_e = Q_1^0 b_1 C_e / (1 + b_1 C_e) + Q_2^0 b_2 C_e / (1 + b_2 C_e)$							
CNT	$Q_1^0$	p of $Q_1^0$	$b_1$	p of $b_1$	$Q_2^0$	p of $Q_2^0$	$b_2$	p of $b_2$
MWCNT20	99	< 0.01	0.486	< 0.01	307000	1	0.000	1.00

\* $q_e$  (mg/g) is equilibrium sorbed concentration;  $C_e$  (mg/L) is equilibrium solution phase concentration.  $Q^0$  (mg/g) is the maximum monolayer adsorption capacity. b constant is related to the molar heat of adsorption.  $K_d$  (L/g) is partition coefficient

**TABLE S2**  
**EXPERIMENTAL AND THEORETICAL MODULI ES OF JCTx (X FROM 10 TO 40) AND THE PARAMETERS INVOLVED IN EQUATION (1).**

	Experimental E (MPa)	Calculated <sup>a</sup> E (MPa)	Density <sup>b</sup> D (g/ml)	Volume fraction <sup>c</sup> $\phi_f$ (%)	Mass fraction $p$ (%)	Parameter $f^d$
JTA	0.3	----	1.17	-----	----	-----
JCT10	1.15	0.69	1.20	0.08	0.1	0.17
JCT15	1.73	0.94	1.21	0.12	0.15	0.21
JCT20	2.01	1.52	1.24	0.16	0.2	0.25
JCT25	2.98	3.02	1.25	0.21	0.25	0.29
JCT30	3.9	5.07	1.27	0.25	0.3	0.33
JCT35	7.54	9.03	1.29	0.30	0.35	0.36
JCT40	13.5	13.5	1.30	0.34	0.4	0.39

<sup>a</sup> modulus E was calculated from eqn (1) based on a  $E_f$  of 85.6 Mpa formulated from fitting modulus of JCT40 into eqn (1). calculated the tensile modulus of composites with co-continuous morphology.

<sup>b</sup> densities of JTA was determined from the buoyancy method, by which JTA was placed in gradient of liquids of known density to approach the density. And the density of composites JCTx were from:  $D=DJTA\rho_{JTA}+DCNT\rho_{CNT}$ , where DCNT and DJTA are densities of MWCNT and JTA, respectively and PCNT and PJTA are mass fraction of MWCNT and JTA, respectively.

<sup>c</sup> Volume fraction =  $(WCNT/DCNT)/(WCNT/DCNT+WJTA/DJTA)$ , where WCNT and WJTA are weights of MWCNT and JTA.

**TABLE S3**  
**EXPERIMENTAL AND THEORETICAL CONDUCTIVITIES OF JCTx (X FROM 1 TO 96) AND THE RELATED PARAMETERS USED IN FITTING EQN (4).**

	Resistivity ( $\Omega.m$ )	Conductivity $\sigma$ ( $S.m^{-1}$ )	$\ln\sigma$	volumn fraction $\phi_f$ (%)	$\ln\phi_f$
JTA	----	-----	-----	----	-----
JCT1	$8.33 \times 10^2$	$1.2 \times 10^{-3}$	-2.92	0.008	-4.76
JCT10	$1.4 \times 10^1$	$7.14 \times 10^{-2}$	-1.15	0.083	-2.49
JCT20	1.02	$9.84 \times 10^{-1}$	-0.01	0.162	-1.82
JCT30	$3.12 \times 10^{-2}$	$3.2 \times 10^1$	1.51	0.236	-1.44
JCT40	$1.53 \times 10^{-3}$	$6.55 \times 10^2$	2.82	0.307	-1.18
JCT50	$3.31 \times 10^{-4}$	$3.02 \times 10^3$	3.48	0.375	-0.98
JCT60	$1.10 \times 10^{-4}$	$9.15 \times 10^3$	3.96	0.439	-0.82
JCT70	$1.48 \times 10^{-5}$	$6.76 \times 10^4$	4.83	0.499	-0.69
JCT80	$2.89 \times 10^{-6}$	$3.46 \times 10^5$	5.54	0.558	-0.58
JCT90	$1.20 \times 10^{-6}$	$8.31 \times 10^5$	5.91	0.613	-0.489
JCT96	$8.26 \times 10^{-7}$	$1.21 \times 10^6$	6.08	0.646	-0.44